J Indian Soc Remote Sens (June 2017) 45:451–462
DOI 10.1007/s12524-016-0613-2

RESEARCH ARTICLE

Local Contrast Based Adaptive SAR Speckle Filter

Sanjay Shitole[1] · Mayank Sharma[2] · Shaunak De[1] · Avik Bhattacharya[1] · Y. S. Rao[1] · B. Krishna Mohan[1]

Received: 20 March 2014 / Accepted: 25 December 2014 / Published online: 28 July 2016

Abstract In this paper, we propose an adaptive filtering technique for Synthetic Aperture Radar (SAR) images. A new windowing technique is introduced where the total window is divided into five equal sized overlapping sub-windows. The pixel to be filtered is a part of each of these sub-windows. A weighted mean of all sub-windows is computed for the pixel under consideration. The weights are accounted from a measure of heterogeneity calculated for each sub-windows. The filter is able to adapt automatically and adjust the speckle suppression strength based on local statistics. This allows the filter to preserve edges while strongly suppressing speckle over homogeneous areas. The proposed filter was compared with some well known SAR filtering techniques in terms of speckle suppression and edge preservation ability. Several experiments were performed on datasets acquired from both air-borne and space-borne SAR platforms. Some well known indices were used for quantitative comparison with other filters. Among the filters compared, the proposed filter shows good speckle suppression ability while still exhibiting reasonable edge preservation ability.

Keywords Speckle · Speckle filter · Synthetic aperture radar (SAR)

✉ Sanjay Shitole
sanjayshitole@iitb.ac.in

Mayank Sharma
mayanksharma.iitb@gmail.com

Shaunak De
shaunakde@iitb.ac.in

Avik Bhattacharya
avikb@csre.iitb.ac.in

Y. S. Rao
ysrao@csre.iitb.ac.in

B. Krishna Mohan
bkmohan@csre.iitb.ac.in

[1] Centre of Studies in Resources Engineering, Indian Institute of Technology Bombay, Mumbai 400076, India

[2] Department of Civil Engineering, Indian Institute of Technology Bombay, Mumbai 400076, India

Introduction

Active microwave remote sensing technology is widely used for Earth-resource observations (Jensen 2009). Synthetic aperture radar (SAR) is the best example of active microwave systems. When a radar illuminates a surface that is rough on the scale of radar wavelength, the return signal consists of waves reflected from many elementary scatterers within a resolution cell. The distances between the elementary scatterers and the receiver vary due to the surface roughness. Therefore, the received waves, although coherent in frequency are no longer coherent in phase. A strong signal is received if the waves add constructively and a weak signal if the waves are out of phase. A SAR image is formed by coherently processing the returns from successive radar pulses. This effect causes a pixel to pixel variation in intensity and this variation manifests itself as a granular pattern called speckle. Speckle in SAR images appear because of the coherent interference of waves reflected from distributed targets (Novak and Burl 1990). Speckle effect in SAR data influences visibility of distributed targets and complicates separation between them. It degrades performance of SAR data analysis techniques and information extraction (Shitole et al. 2013, 2014). Speckle also alters the visual information that is critical to applications such as mapping and segmentation. Speckle is

signal dependent granular noise and its removal is difficult because of its multiplicative nature. Multi-look processing is widely used for speckle reduction. Multi-look based approach causes decrease in spatial resolution of data. To overcome this problem several speckle filtering algorithms have been developed (Sumantyo and Amini 2008).

Development of adaptive speckle reduction techniques is the research problem for the last 30 years. Two approaches may be taken for speckle reduction, multi-look processing and Posterior processing. In multi-look processing subsequent pulses of the radar are processed independently to create several SAR images of the same ground area, called SAR looks (Oliver and Quegan 2004). This is then subsequently combined to form a single SAR image (Porcello et al. 1976), effectively reducing the bandwidth (Moreira 1991). This processing however causes a loss in resolution proportional to the number of looks combined (Martin and Turner 1993). This kind of speckle suppression is performed during the data processing stage and may not be suitable for applications demanding high resolution. For preservation of image resolution or for further speckle reduction, posterior speckle filtering techniques may be applied after image formation. Posterior speckle filtering can be broadly considered in the three approaches: frequency, wavelet and spatial domain filtering.

The Weiner filter (Walkup and Choens 1974) and filters proposed by Li (1988) are based on minimum mean-square error (MMSE) fitting in the frequency domain. Wavelet based filters, derived from the theory on multi-resolution analysis (Mallat 1989a, b) have been proposed. Gagnon and Jouan (1997) proposed a Wavelet Coefficient Shrinkage (WCS) filter which outperforms standard filters for high noise level images. Fukuda and Hirosawa (1998) have proposed a filter that acceptably smoothens homogeneous areas and preserves edges. In (Simard et al. 1998) the analysis of the contribution of speckle noise to the wavelet decomposition of SAR images is performed. SAR image de-noising via Bayesian wavelet shrinkage was shown by Achim et al. (2006). Spatially adaptive wavelet based methods have been demonstrated by Bhuiyan et al. (2007) to good effect.

A method for SAR de-speckling using second generation wavelets (Gleich et al. 2010) has the ability to preserve texture features in the image.

Compared to frequency domain, adaptive spatial domain filters such as Lee, Frost, Lee-sigma, gamma-map are widely used (Sumantyo and Amini 2008). All these speckle filters improve the visibility of distributed targets in a given data. We require simple, efficient, and adaptive speckle reducing techniques to process SAR images. Ideally, speckle filters should preserve local mean value, point targets and edges. The Boxcar filter (Mean filter) is a simple averaging filter that replaces the center pixel by the mean value of pixels in a scanning window. The Median filter replaces the center pixel by the median of all pixels in a scanning window. The Boxcar filter and the Median filter do not easily lend themselves to adaptive implementation, especially, the Mean filter (Durand and Perbos 1987). In Lee's Local Statistics (LS) filter, a priori mean and variance is obtained using local statistics (Lee 1980). Then, the noise reduced pixel is estimated using the minimum mean-square error (MMSE) (Lee 1980). The main deficiency of this filter is that speckle noise near strong edges is not adequately filtered. In Frost filter (Frost et al. 1982), the noise in the edge areas is less prominent than for the LS filter, but the edges are somewhat blurred. A Frost filter adapts to the noise variance within the filter window by applying exponentially weighting factors (Lee et al. 1994). The characteristics of this filter is similar to those of the LS filter except in the edge areas where the Frost filter does more averaging (Lee et al. 1994). The focus of the Gamma or Maximum A Posteriori (MAP) filter (Lopes et al. 1990a) is to minimize the loss of texture information by assuming that the image of forested areas, agricultural lands, and oceans are gamma-distributed scenes. The approach used in MAP filter is better than the Frost and LS filter. It uses the coefficient of variation (CV) and contrast ratios, whose theoretical probability density functions will determine the smoothing process. Kuan filter (Kuan et al. 1985) adaptively filters homogeneous and heterogeneous areas. The modified Lee and Kuan filters give similar visual results (Lopes et al. 1990b). To overcome the deficiency of LS filter, the Lee refined filter (Lee 1981) was introduced. In this approach, noise near edges is minimized using edge-aligned windows. Refined Lee filter is adaptive and does not smear edges and subtle details, however its computational complexity is more (Lee et al. 1997). A conceptually simple and effective method based on sigma probability of a Gaussian distribution is proposed by Lee (1983). In this method, pixel values within two noise standard deviations are averaged for speckle reduction. It has deficiencies such as bias in the estimation, unfiltered black pixels and blurring of point targets. Improved Sigma filter (Lee et al. 2009) is an improvement over the Lee sigma filter and modified for target preservation to resolves bias problem. In this filter, sigma range is calculated to remove bias using theoretical speckle distributions. Adaptive despeckling is performed by Achim et al. (2006), by deriving a MAP estimator for the heavy tailed Rayleigh distribution to estimate the Radar Cross Section. Nonlocal (NL) filtering is a promising method for speckle reduction (Deledalle et al. 2009; Parrilli et al. 2012; Gomez et al. 2013). In this method each pixel is weighted according to its similarity with the pixels for speckle reduction. The nonlocal mean filter (Buades et al. 2005) uses the Euclidean distance measure to find the similarity between the patch centered at the pixel under consideration for filtering and patch centered at given neighborhood pixel. It has been

shown that (Iqbal et al. 2013; Ponomaryov 2007) filters derived from the field of compressive sensing have outperformed traditional filters.

A filter cannot be considered to be supreme over another and the strength and limitations of a filter is unique in the context of a specific application (Lee et al. 1994). For large scale image interpretation and mapping a speckle filter which degrades the spatial resolution may be acceptable (Qiu et al. 2004; Xiao et al. 2003). However, it is essential in some applications to preserve the resolution of imagery. In such a situation, an adaptive filter that can preserve fine details like edges while showing good speckle suppression in homogeneous areas is essential. Research community has used the Boxcar filter because of its simplicity, even though it suffers from problems like blurring of edges, point targets and reduction in spatial resolution (Balenzano et al. 2013; Tan et al. 2007; Wang et al. 2013; Yamamoto et al. 2013). In SAR applications filtering is used as a pre-processing step. Even though an abundance of SAR speckle filters available, we see that in recent literature, the Boxcar or Lee filters are employed (Balenzano et al. 2013; Tan et al. 2007; Wang et al. 2013; Yamamoto et al. 2013). Adaptive filters are also employed when preservation of fine details are required. However, these filters require a global threshold as an input parameter. This threshold needs to be determined by experimental study for a L look image. In the proposed filter we do not require any threshold value to be fixed. Rather an adaptive parameter is computed based on local statistics. Over the years a number of speckle filters with high computational complexity have been proposed. Majority of these exhibits a better performance than the mean filter in some aspects, however the increase in performance is not proportional to the added complexity in design and implementation of the filter. In this paper we propose a filter that achieves reasonably good performance compared to the existing ones, while still being comparable in computational efficiency. We use a new directional subset selection based speckle filtering approach where the total filtering window is divided in subwindows to preserve details. The proposed filter is evaluated quantitatively and qualitatively using both air-borne and space-borne data sets of various frequency bands. Experimental results reveals that the proposed SAR speckle filter is comparable and at times better than the established speckle filters with the added benefit of being conceptually simple, adaptive and easy to implement.

Speckle Model

The speckle model assumes that the Earth's surface is rough on the scale of radar wavelength and a resolution cell contains large number of scatterers. The surface roughness cause changes in the amplitude (A) and the phase (ϕ) of reflected electromagnetic (EM) wave in a two-dimensional resolution cell. Each reflected EM wave can be represented as a phasor and the total amplitude is given by the vector summation over N scatterers $\sum_N A_i e^{j\phi_i}$. The measured local reflectivity is represented by the complex number formed by the in-phase $(Acos(\phi))$ and the quadrature components $(Asin(\phi))$ of the amplitude. The in-phase and the quadrature components are independent and identically distributed zero-mean Gaussian variables. The real and the imaginary images are less informative (Sumantyo and Amini 2008) and the phase (ϕ) is completely noise like. Although the amplitude and the intensity ($I = A^2$) images are informative they are degraded by noise. The pixel to pixel intensity variation in images which is granular in nature is referred to as speckle. The multiplicative nature of speckle affects brighter pixels more than darker pixels. The standard deviation of speckle is proportional to the mean and so it is often modelled as a multiplicative process. This model has led to a number techniques for SAR image processing and analysis. The multiplicative model states that the observation of a single pixel is a random variable $Z : \Omega \rightarrow \mathbb{R}^+$. The model is a product of two independent random variables, $X : \Omega \rightarrow \mathbb{R}^+$ is the speckle noise component with unit mean and $Y : \Omega \rightarrow \mathbb{R}^+$ is the true observed reflectivity. The distribution of Z depends on the distribution of X and Y. Many univariate and multivariate distributions have been proposed in the literature (Frery et al. 1997; Yueh et al. 1989) to characterize the distribution of the return Z. The speckle noise is Γ distributed as,

$$p_X(x) = \frac{L^L}{\Gamma(L)} x^{L-1} exp(-Lx), \quad L, x > 0 \tag{1}$$

where L is the number of looks which is used to improve the estimate of the mean intensity. A efficient speckle filter would tend to increase this parameter referred to as the number of looks. The exponential distribution is a good model for 1-look SAR intensity image whereas the Chi-square distribution of $2L$ degrees of freedom serves as good model for a L look SAR intensity image. These models are valid under the assumptions that the scene under consideration is a homogeneous area characterized by distributed targets devoid of the presence of any point target. The strong reflectivity from a single point target in a resolution cell is characterized by the Rice distribution.

The Proposed Filter

In general a filtering operation involves averaging of pixels in a window distributed equally around the central pixel. Due to this a high contrast area or edge present in one subset of the neighborhood of the central pixel spreads to

other subsets where it was originally not present. This windowing operation leads to edge blurring. In (Lee 1981) a new directional subset selection based filtering method was proposed to incorporate the local gradient information to improve edge preservation. In this work we use a sub-window based approach to prevent high contrast areas or edges present in one subset of the neighborhood from spreading to other subsets. The most commonly used Boxcar (i.e. mean) filter enhances the radiometric resolution at the cost of spatial resolution. In this process the images gets blurred and edges are smeared out. Suitable neighborhood information is utilized in this work in order to preserve subtle details in the image while removing speckle. The proposed filter defines a new filtering neighborhood structure.

The total filter mask is divided into five sub-windows as shown in Fig. 1. Each sub-window contains the central pixel of the total mask (the pixel to be filtered) as one of its element. This neighborhood structure makes the filter more adaptive for single targets, edges and homogeneous regions.

In general if n is the size of each sub-window then the total filter mask will be of size $2N-1$ (eg. If $n=3$ for each sub-window then $2N-1=5$ is the total mask size). The quadratic corner difference (QCD) of a ith sub-window is defined in Eq. (2) as,

$$QCD_i = \sqrt{\frac{1}{N^2}\sum_{k=1}^{N^2}(x_k^i - I_c)^2} \tag{2}$$

where x_k^i is the value of the kth pixel in the ith sub-window and I_c is the central pixel value of the total mask. The final filtered value R is obtained for a mask of size $2N-1$ as shown in Eq. (3),

$$R = \frac{\sum_{i=1}^{5}\mu_i\left(\frac{1}{QCD_i}\right)^{\eta}}{\sum_{i=1}^{5}\left(\frac{1}{QCD_i}\right)^{\eta}} \tag{3}$$

where μ_i is the mean of the ith sub-window. The sub-window configuration along with the inverse QCD incorporates feature preservation while the mean does the smoothing. The exponent η determines the ability of the performance of the filter to adapt to the window under consideration. For homogeneous areas η needs to be a low value to allow maximum smoothing (Boxcar filtering) whereas to preserve edges the value of η must be large (η_{max}). The value of η is obtained from the model given in Eq. (4),

$$\eta = \eta_{max}\left(1 - e^{-\sigma^2(QCD_i)}\right) \tag{4}$$

It is assumed that in heterogeneous areas the variance of the $QCD's$ $(\sigma^2(QCD_i))$ will be large and hence η will tend to η_{max}. In homogeneous areas conversely the variance of $QCD's$ will be small and hence η will be very small. Multiple trails were run with varying η on homogeneous and heterogeneous areas from several images acquired with different sensors with varying resolutions. It was found that with increasing values of η the coefficient of variation (CV) for a homogeneous area of the test data slightly increases initially, but for values of $\eta > \eta_{max}$, no appreciable change in CV is observed and hence the maximum value of η is limited to η_{max}. It was experimentally determined that the value of $\eta_{max}=5$ is sufficient to preserve edges and perform filtering of homogeneous areas.

Quantitative analysis of the performance of the filter in comparison to some of the existing filters are performed on real SAR data. Some indices commonly used to evaluate the performance of SAR filters are used in this study. The results of the analysis and a brief description of the indices are treated in the next section. The algorithm for the proposed speckle filter is listed in "Appendix".

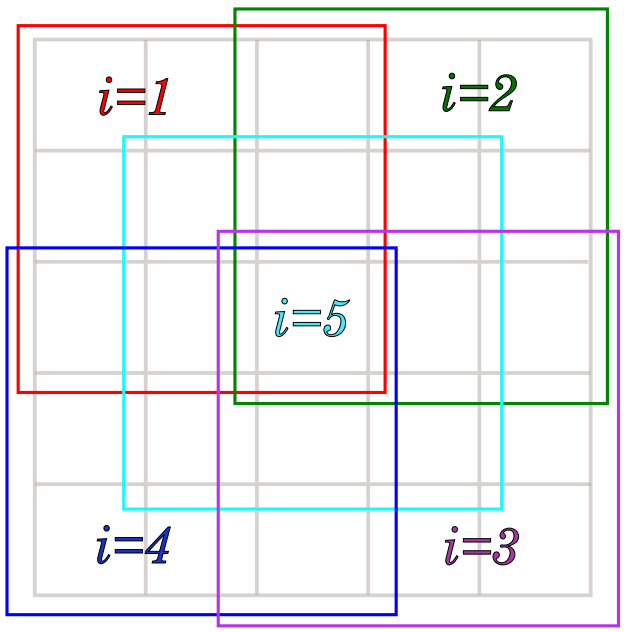

Fig. 1 Five sub-window mask for the proposed filter

Experimental Results

The performance of the filter was evaluated on dataset acquired from both air-borne and space-borne SAR systems of various frequency bands. The air-borne dataset was comprised of a C-band AIRSAR image acquired over Felvoland, Netherlands and an L-band UAVSAR image acquired over Winnipeg, Canada. Both these scenes primarily consists of agricultural areas with well-defined field boundaries. The AIRSAR image contains a series of corner reflectors that were used for evaluating the performance of

the filter over single target. The space-borne dataset was comprised of a X-band TerraSAR-X Spotlight image acquired over Vishakhapatnam, India,

The filtered images were visually inspected followed by quantitative comparison with other filters. For this we have used commonly used assessment measures like Equivalent Number of Looks (ENL), Edge Save Index in Horizontal (ESIH), Edge Save Index in Vertical (ESIV) direction, mean and standard deviation of the ratio image. The ENL is used to evaluate the smoothing level in homogeneous areas (Lee 1981). The variations in homogeneous regions are assumed to be less compared to variation in the speckle intensity. As the smoothing capacity of speckle filter improves, the ENL increases. The ESIH and ESIV reflects edge preservation capability of the speckle filter and should be unity for an ideal filter (Iqbal et al. 2013). The ratio image is obtained by the pixel by pixel division of the input and the filtered image (Argenti et al. 2013). For an ideal filter, this ratio represents a Γ distributed noise that must be removed. Mean of the ratio image should be close to unity and the standard deviation should match that of the speckle model.

Table 1 Evaluation of speckle filters for the AIRSAR C-band data using equivalent number of looks (ENL), edge preservation index in vertical and horizontal direction (ESIV, ESIH) and ratio image

	ENL	ESIV	ESIH	Ratio image	
				Mean	SD
Boxcar filter	8.81	0.25	0.24	1.00	0.32
Proposed filter	8.47	0.28	0.28	0.99	0.26
Frost ($k = 0.5$)	8.76	0.36	0.35	0.97	0.31
Frost ($k = 2$)	8.58	0.45	0.43	0.97	0.30
Lee filter	6.75	0.67	0.43	0.98	0.13

AIRSAR C-band Flevoland, Netherlands

The image is of an agricultural area with an array or corner reflectors set up in the central field. The Boxcar, proposed, Frost ($k = 0.5$ and $k = 2$), Lee filter are applied with a 5×5 window on a AIRSAR C-band dataset. From Table 1 it can be seen that the ENL of the proposed filter is 8.47 which is comparable to the Boxcar (8.81), Frost ($k = 0.5$) (8.76), Frost ($k = 2$) (8.58). The Lee filter has a lower ENL of 6.75

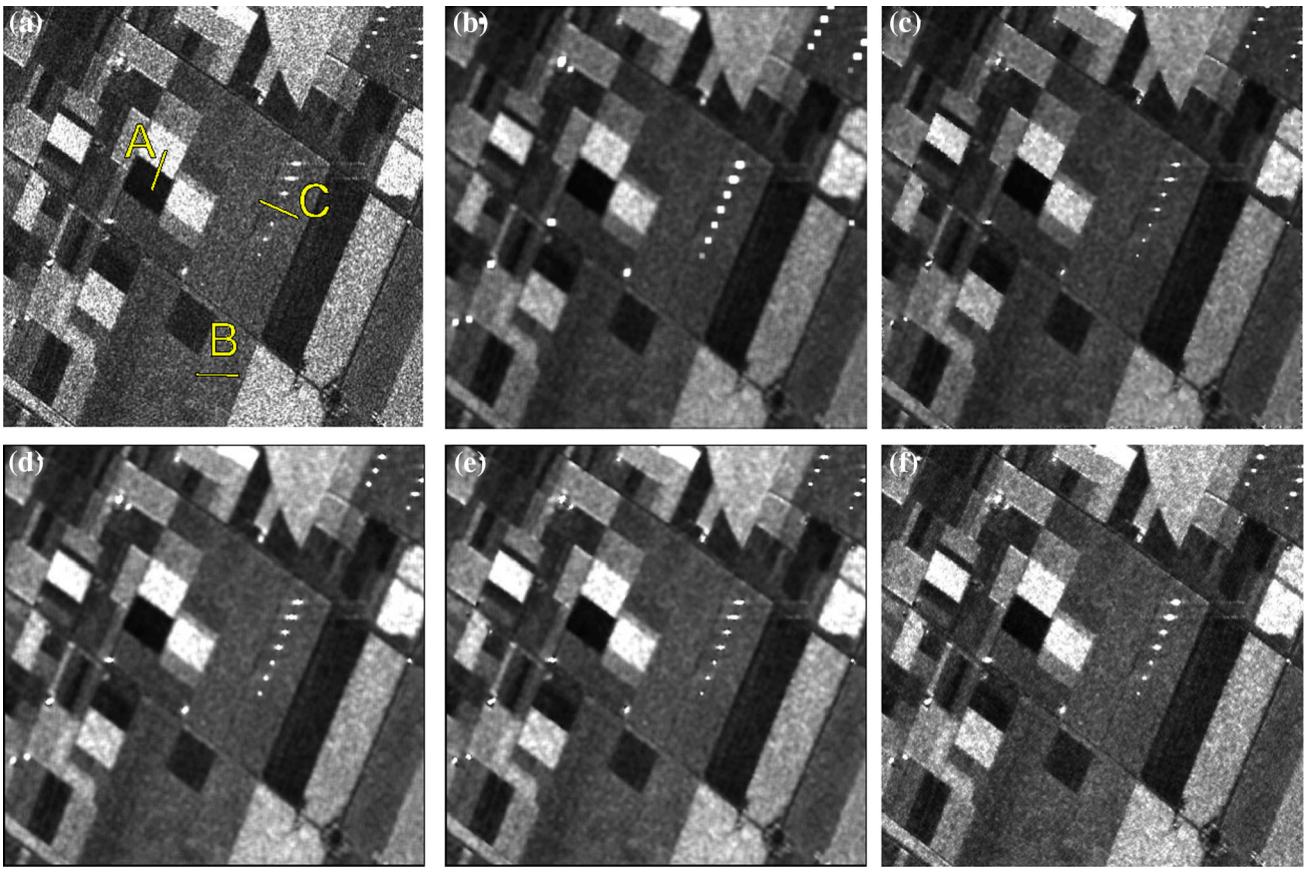

Fig. 2 Speckle filtering results using AIRSAR C-band data acquired over Flevoland, Netherlands. **a** Original unfiltered data (*Transect lines* for profile plots are visible where profile *A* represents edge, *B* represents homogeneous area and *C* represents a single target), **b** Boxcar filter, **c** Proposed filter, **d** Frost filter ($k = 0.5$), **e** Frost filter ($k = 2$), **f** Lee filter

Table 2 Evaluation of speckle filters for the UAV SAR L-band data using equivalent number of looks (ENL), edge preservation index in vertical and horizontal direction (ESIV, ESIH) and ratio image

	ENL	ESIV	ESIH	Ratio image	
				Mean	SD
Boxcar filter	38.51	0.18	0.19	0.98	0.53
Proposed filter	32.74	0.22	0.24	0.97	0.43
Frost ($k = 0.5$)	35.84	0.21	0.24	0.95	0.45
Frost ($k = 2$)	23.43	0.37	0.43	0.95	0.35
Lee filter	9.92	0.59	0.43	0.94	0.20

but however has better edge preserving capability. The ESIV and ESIH for the proposed filter is 0.28 which is better than the Boxcar but less than Frost ($k = 0.5$ and $k = 2$). As noted previously the Lee filter has a good edge preservation performance but at the cost of poor smoothing of homogeneous areas. Mean and standard deviation calculated from ratio image for the proposed filter is 0.99 while the standard deviation is 0.26 which is comparable to the other filters.

Profile plots are presented to highlight the filtering and edge-saving ability of the proposed filter. Profile plot for transect *A* is shown in Fig. 2a from a homogeneous area in the AIRSAR image. The proposed and the Frost ($k = 0.5$

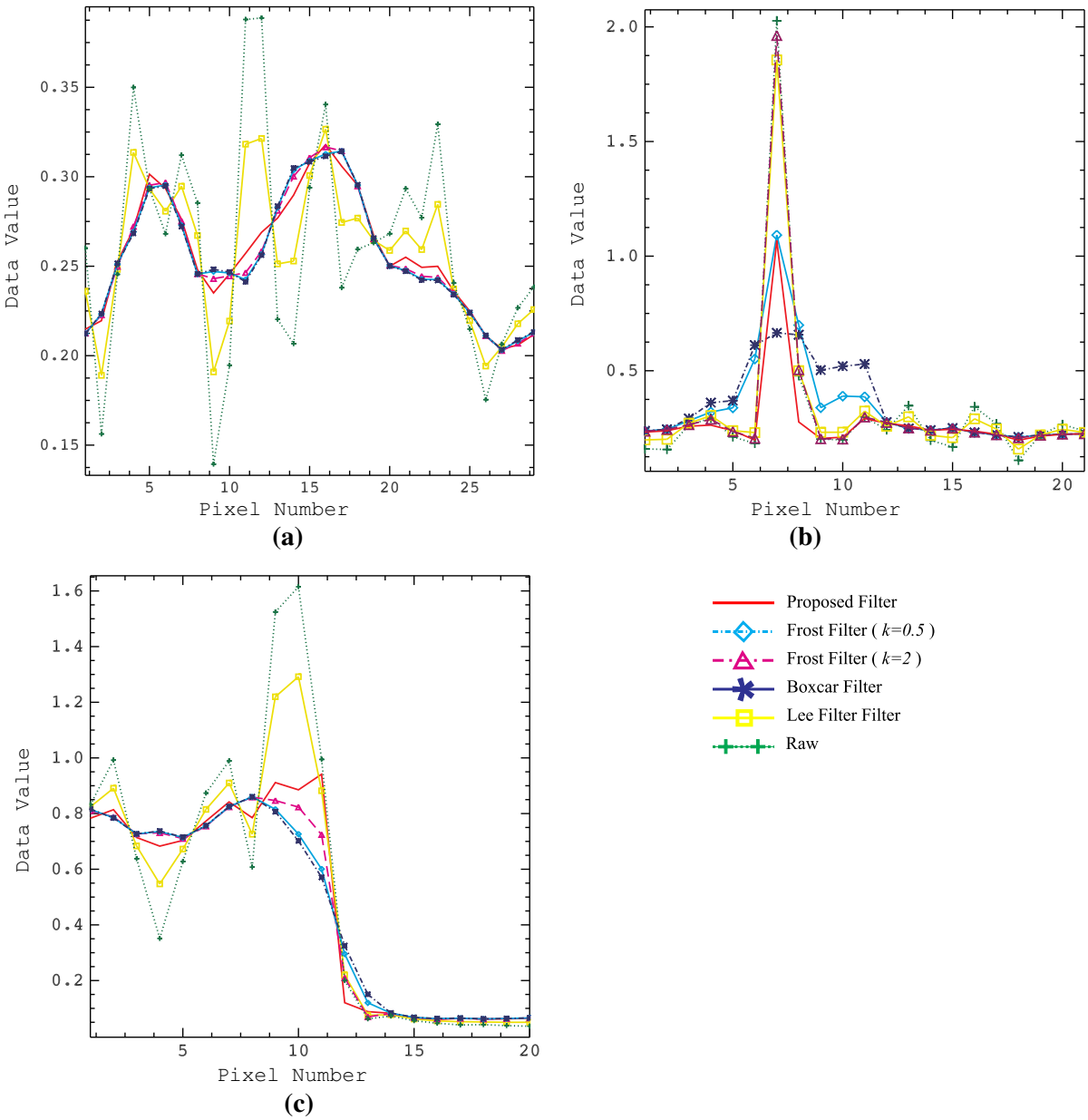

Fig. 3 Profile plots for the AIRSAR C-band image acquired over Flevoland **a** homogeneous area, **b** single target, **c** edge. Profile plots are obtained from the transects shown on (Fig. 2a)

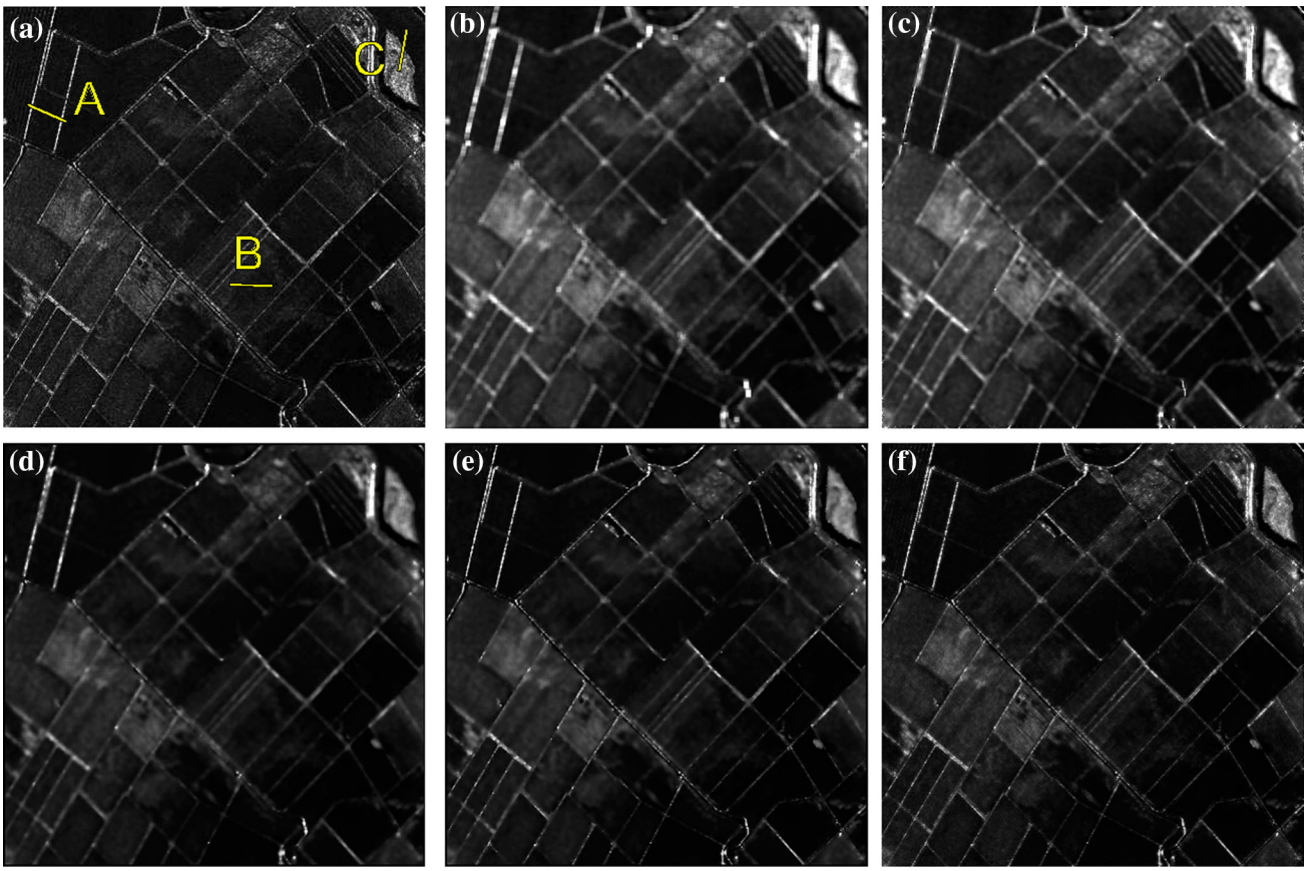

Fig. 4 Speckle filtering results using UAV SAR L-band. **a** Original unfiltered data, **b** Boxcar filter, **c** Proposed filter, **d** Frost filter ($k = 0.5$), **e** Frost filter ($k = 2$), **f** Lee filter

and $k = 2$) filter follow the Boxcar filter. The Lee filter bears a greater resemblance to the raw data itself. It has a higher variation even in this homogeneous area and hence has a poorer ENL as compared to other filters. A profile transect from a single target is shown in Fig. 2b marked by profile plot C. As we know the single (point) target does not follow the multiplicative noise assumption. So ideally there should be no effect of filtering on such targets, the value should be preserved. The worst case scenario is Boxcar filter where this value is seriously affected. Lee filter preserves this value while Frost, with adjusted damping factor follows a similar trend to the single target. The proposed filter behaves similar to the Frost filter but does not require *a priori* information about the damping factor. Profile plot from an edge in the image is shown in Fig. 2c by transect *B*. The proposed and Lee filter follows the edge in the original image better than the others as shown in Fig. 3.

UAVSAR L-band Winnipeg, Canada

The image is acquired over agricultural regions with well defined boundaries as shown in Fig. 4. The quantitative results for UAVSAR L-band data are shown in Table 2. The proposed filter with ENL of 32.74 shows a better smoothing capacity than Lee filter (ENL = 9.92) and comparable with Frost ($k = 0.5$) with ENL of 35.84. However, the proposed filter has a better edge preservation ability than the Frost ($k = 0.5$) as illustrated by the profile plot shown in Fig. 5c. When the damping factor (k) is set to 2 for the Frost filter, the edge preservation property is improved but at the cost of it's smoothing ability. The ENL drops by 35 % from 35.84 (for $k = 0.5$) to 23.43 (for $k = 2$). Profile plots for two parallel edges in the image are shown in Fig. 5a. The proposed filter shows negligible blurring of the edges. The profile lies completely within that of the original image for the proposed and the Lee filter whereas the Frost ($k = 0.5$) tends to blur the edges. However, in homogeneous areas the Lee filter shows a lot of variance and lower smoothing ability than the proposed filter as shown in Fig. 5b. Mean value obtained from ratio image for the proposed filter is better than the Frost and Lee filter. The proposed filter shows a value of 0.97 which is comparable to the Boxcar, Lee and Frost ($k = 0.5$ and $k = 2$) which show a mean of 0.98, 0.94, 0.95 and 0.95 respectively. The standard deviation of the ratio image is

comparable to Boxcar, proposed and Frost ($k = 0.5$) however this value is low for Lee and Frost ($k = 2$) filter.

TerraSAR-X X-band Visakhapatnam, India

The image is acquired over a busy port in the south of India. We have selected an area which contains the major roadway leading upto the port. Speckle filtering results for TerraSAR-X band data are tabulated in Table 3. Smoothing capability of the proposed filter (ENL = 10.22) is better than Lee (ENL = 4.09) and Frost filter ($k = 2$) (ENL = 6.82). and is comparable with Frost filter ($k = 0.5$) (ENL = 10.77) and Boxcar (ENL = 11.66). Edge preservation capability of proposed filter is better as compared to Frost ($k = 0.5$) but less than the Lee and Frost filter ($k = 2$). Ratio image mean value is 0.96 for the proposed filter which is slightly better than Lee (0.90), Frost ($k = 0.5$) and Frost filter ($k = 2$) at 0.94 and 0.92 respectively. Standard deviation of ratio image is lower for Lee filter compared to Frost and proposed filter. The profile plots for two transects are marked in Fig. 6a. Homogeneous area, represented by

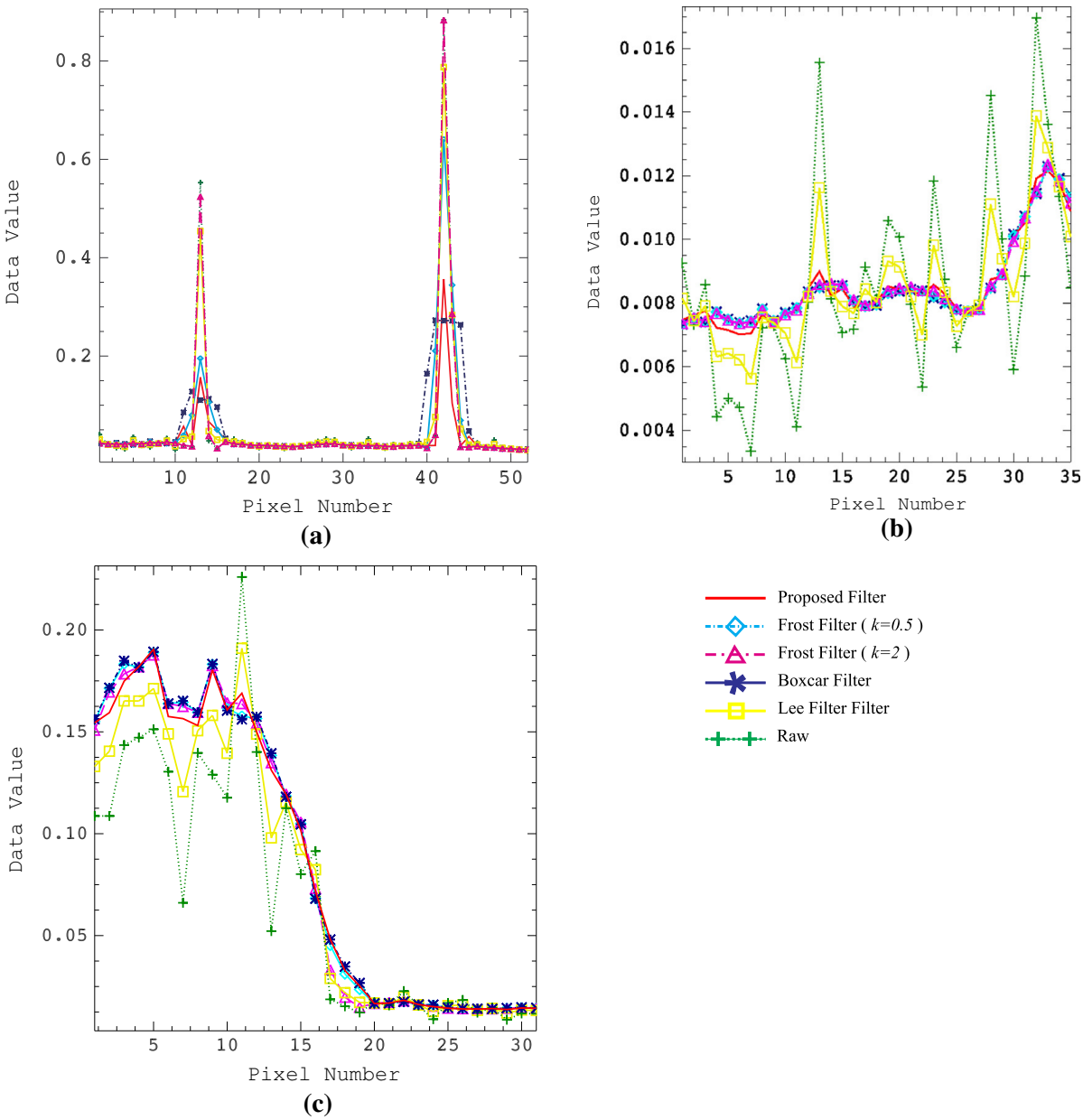

Fig. 5 Profile plot for the UAV SAR L-band image. **a** Two parallel edges, **b** homogeneous area, **c** edge, **d** legends used in Figs. 3 and 5. Profile plots are obtained from the transects shown on Fig. 4a

Table 3 Evaluation of speckle filters for the TerraSAR-X X-band data using equivalent number of looks (ENL), edge preservation index in vertical and horizontal direction (ESIV, ESIH) and ratio image

	ENL	ESIV	ESIH	Ratio image	
				Mean	SD
Boxcar filter	11.66	0.16	0.16	0.98	0.69
Proposed filter	10.22	0.21	0.21	0.96	0.55
Frost filter ($k = 0.5$)	10.77	0.18	0.17	0.94	0.61
Frost filter ($k = 2$)	6.82	0.31	0.32	0.92	0.45
Lee filter	4.09	0.60	0.32	0.90	0.27

transect B, is shown in Fig. 7a. We see that the Lee filter shows variations even in homogeneous areas whereas the other filters show better smoothing. The plot for edge transect A is shown in Fig. 7b. The Lee and the Frost ($k = 2$) rise sharply in accordance to the unfiltered data at the edges. Although the proposed filter has a lower rise in intensity, it is able to well preserve the profile of the edge.

The computational efficiency of the proposed speckle filter is shown in Table 4. It can be observed that the proposed speckle filter is computationally comparable to other filters when tested for a 1000×1000 image on an intel i5 machine (2.2 GHz) with 4 GB of RAM.

Conclusion

The proposed filter is able to provide maximum speckle suppression in homogeneous areas while still showing good edge preservation. Several examples of this have been presented in this study. The Frost filter offer a damping factor parameter that affords a choice between the speckle suppression capability and the edge preservation ability. It performs greater smoothing when $k = 0.5$ and more edge preservation when $k = 2$. The proposed filter is comparable to Frost ($k = 0.5$) in terms of speckle smoothing ability and Frost ($k = 2$) in edge preservation ability. It is noted that the Lee filter performs poorly in terms of smoothing in homogeneous areas, but has the best edge preservation.

This edge preservation ability is largely due to the adaptive nature of the filter which used a edge prediction model to automatically adjust the smoothing strength of the filtering process. The Lee and the Frost filters require a global threshold parameter to be fixed for an L look image.

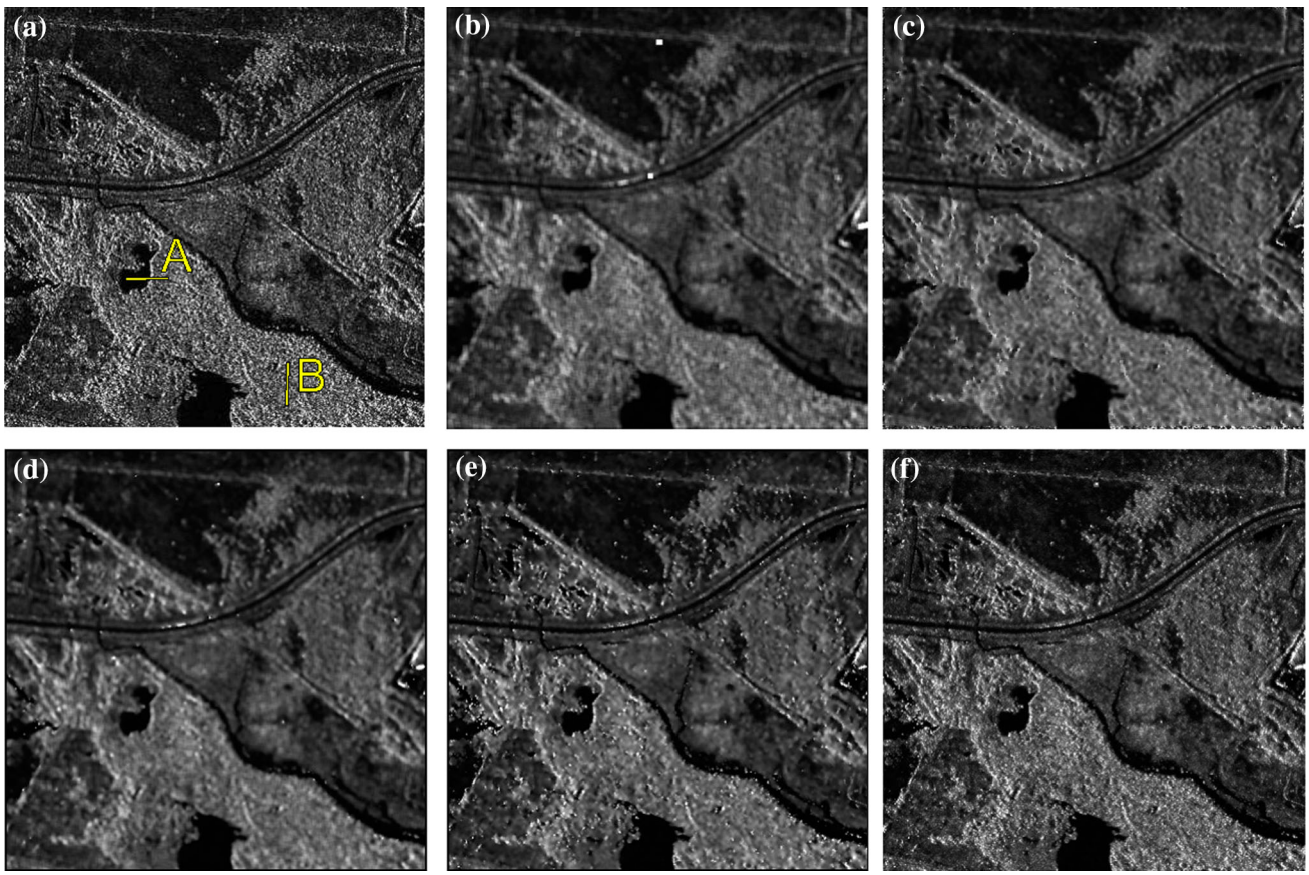

Fig. 6 Speckle filtering results using TerrSAR-X X-band data. **a** Original unfiltered data (*Transect lines* for profile plots are visible where profile *A* represents edge and *B* represents homogeneous area). **b** Boxcar filter, **c** Proposed filter, **d** Frost filter ($k = 0.5$), **e** Frost filter ($k = 2$), **f** Lee filter

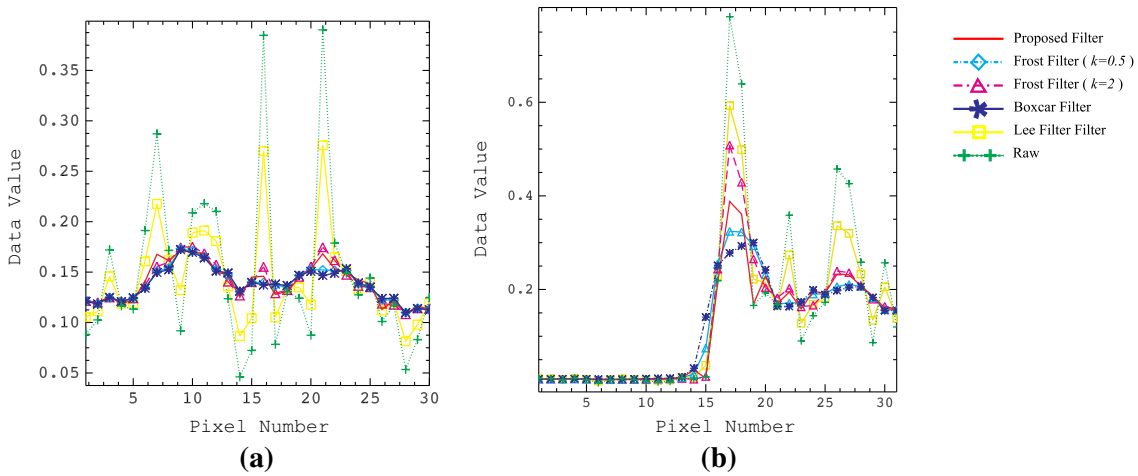

Fig. 7 Profile plot for the TerraSAR X-band image. **a** Homogeneous area, **b** edge, **c** legends. Profile plots are obtained from the *transects* shown on Fig. 6a

Table 4 Comparison of the computation time for filters

Speckle Filter	Time (s)
Boxcar	4.21
Proposed filter	4.81
Frost ($k = 0.5$)	5.31
Frost ($k = 2$)	5.31
Lee filter	4.71

This parameter need to be experimentally determine beforehand. The proposed filter does not require a global parameter to be input, but rather computes the adaptive parameter (η) and adjusts it based upon local statistics. At higher values of η, point targets and edges are preserved while at lower values of η greater smoothing is obtained. Computationally, the proposed filter is simple and depends only on local statistics. Consequently each pixel can be processed independent of other pixels, allowing the implementation of parallelism techniques for fast processing. The mean value calculated from the ratio of the filtered and original images are closer to unity as compared to the Lee and Frost filter, indicating that the bias is lowest for the proposed method.

The proposed filter has been shown on various datasets from different platforms and has been found to be suitable for speckle suppression, mean preservation and edge saving.

Acknowledgments The authors would like to thank NASA/JPL-Caltech for providing sample imagery of UAVSAR and AIRSAR used in this work. TerraSAR-X sample dataset is courtesy of Astrium GEO-Information Services.

Algorithm 1:

Input: Intensity Image (I)
Output: Filtered Intensity Image (R)
Data: $n \leftarrow$ Sub-window Size

begin
  $N \leftarrow 2n-1$
  for $i \leftarrow 0$ **to** *number of rows* **do**
    for $j \leftarrow 0$ **to** *number of columns* **do**
      Consider pixel $I(i,j)$
      Select $N \times N$ total window around $I(i,j)$
      Select 5 sub-windows $s.t.$:
        Window 1 (NW):
        $i : (i-n, i]$ *and* $j : (j-n, j]$
        Window 2 (NE):
        $i : [i, i+n)$ *and* $j : (j-n, j]$
        Window 3 (SE):
        $i : (i-n, i]$ *and* $j : [j, j+n)$
        Window 4 (SW):
        $i : [i, i+n)$ *and* $j : [j, j+n)$
        Window 5 (Central):
        $i : [i-\frac{n}{2}, i+\frac{n}{2}]$ *and* $j : [j-\frac{n}{2}, j+\frac{n}{2}]$
      for $k \leftarrow 1$ **to** 5 **do**
        $wm_k \leftarrow f(QCD_k, \eta_k)$
      end
      $R(i,j) \leftarrow \sum_{k=1}^{k=5} wm_k$
    end
  end
end
NW = North West, NE = North East, SW = South West, SE = South East

Appendix

Algorithm for the proposed filter is presented here.

References

Achim, A., Kuruoglu, E., & Zerubia, J. (2006). SAR image filtering based on the heavy-tailed rayleigh model. *IEEE Transactions on Image Processing*, *15*, 2686–2693. doi:10.1109/TIP.2006.877362.

Argenti, F., Lapini, A., Bianchi, T., & Alparone, L. (2013). A tutorial on speckle reduction in synthetic aperture radar images. *IEEE Geoscience and Remote Sensing Magazine*, *1*, 6–35.

Balenzano, A., Satalino, G., Lovergine, F., Rinaldi, M., Iacobellis, V., Mastronardi, N., et al. (2013). On the use of temporal series of L-and X-band SAR data for soil moisture retrieval. Capitanata plain case study. *European Journal of Remote Sensing*, *46*, 721–737.

Bhuiyan, M. I. H., Ahmad, M., & Swamy, M. (2007). Spatially adaptive wavelet-based method using the cauchy prior for denoising the SAR images. *IEEE Transactions on Circuits and Systems for Video Technology*, *17*, 500–507.

Buades, A., Coll, B., & Morel, J. M. (2005). A non-local algorithm for image denoising. In *IEEE computer society conference on computer vision and pattern recognition, 2005. CVPR 2005* (Vol. 2, pp. 60–65).

Deledalle, C.-A., Denis, L., & Tupin, F. (2009). Iterative weighted maximum likelihood denoising with probabilistic patch-based weights. *IEEE Transactions on Image Processing*, *18*, 2661–2672.

Durand, J. M. G. B. J., & Perbos, J. R. (1987). SAR data filtering for classification. *IEEE Transactions on Geoscience and Remote Sensing*, *GE–25*, 629–637.

Frery, A., Muller, H.-J., Yanasse, C., & Sant'Anna, S. (1997). A model for extremely heterogeneous clutter. *IEEE Transactions on Geoscience and Remote Sensing*, *35*, 648–659. doi:10.1109/36.581981.

Frost, V. S., Stiles, J. A., Shanmugan, K. S., & Holtzman, J. (1982). A model for radar images and its application to adaptive digital filtering of multiplicative noise. *IEEE Transactions on Pattern Analysis and Machine Intelligence*, *PAMI–4*, 157–166. doi:10.1109/TPAMI.1982.4767223.

Fukuda, S., & Hirosawa, H. (1998). Suppression of speckle in synthetic aperture radar images using wavelet. *International Journal of Remote Sensing*, *19*, 507–519. doi:10.1080/014311698216125.

Gagnon, L., & Jouan, A. (1997). Speckle filtering of SAR images: A comparative study between complex-wavelet-based and standard filters. In *Optical Science, Engineering and Instrumentation'97* (pp. 80–91). International Society for Optics and Photonics

Gleich, D., Kseneman, M., & Datcu, M. (2010). Despeckling of TerraSAR-X data using second-generation wavelets. *IEEE Geoscience and Remote Sensing Letters*, *7*, 68–72.

Gomez, L., Munteanu, C. G., Buemi, M. E., Jacobo-Berlles, J. C., & Mejail, M. E. (2013). Supervised constrained optimization of bayesian nonlocal means filter with sigma preselection for despeckling sar images. *IEEE Transactions on Geoscience and Remote Sensing*, *51*, 4563–4575.

Iqbal, M., Chen, J., Yang, W., Wang, P., & Sun, B. (2013). SAR image despeckling by selective 3D filtering of multiple compressive reconstructed images. *Progress In Electromagnetics Research*, *134*, 209–226.

Jensen, J. R. (2009). *Remote sensing of the environment: An earth resource perspective*, 2 edn. New Delhi: Dorling Kindersley.

Kuan, D. T., Sawchuk, A., Strand, T. C., & Chavel, P. (1985). Adaptive noise smoothing filter for images with signal-dependent noise. *IEEE Transactions on Pattern Analysis and Machine Intelligence*, *PAMI–7*, 165–177. doi:10.1109/TPAMI.1985.4767641.

Lee, J., Grunes, M., & De Grandi, G. (1997). Polarimetric SAR speckle filtering and its impact on classification. In *Geoscience and remote sensing. IGARSS '97. Remote sensing—a scientific vision for sustainable development, 1997 IEEE. International* (Vol. 2, pp. 1038–1040).

Lee, J. S. (1980). Digital image enhancement and noise filtering by use of local statistics. *IEEE Transactions on Pattern Analysis and Machine Intelligence*, *PAMI–2*, 165–168.

Lee, J. S. (1981). Refined filtering of image noise using local statistics. *Computer Graphics and Image Processing*, *15*, 380–389.

Lee, J. S. (1983). A simple speckle smoothing algorithm for synthetic aperture radar images. *IEEE Transactions on Systems, Man and Cybernetics*, *SMC–13*, 85–89. doi:10.1109/TSMC.1983.6313036.

Lee, J. S., Jurkevich, L., Dewaele, P., Wambacq, P., & Oosterlinck, A. (1994). Speckle filtering of synthetic aperture radar images: A review. *Remote Sensing Reviews*, *8*, 313–340.

Lee, J. S., Wen, J. H., Ainsworth, T. L., Chen, K. S., & Chen, A. J. (2009). Improved sigma filter for speckle filtering of SAR imagery. *IEEE Transactions on Geoscience and Remote Sensing*, *47*, 202–213.

Li, C. (1988). Two adaptive filters for speckle reduction in SAR images by using the variance ratio. *International Journal of Remote Sensing*, *9*, 641–653.

Lopes, A., Nezry, E., Touzi, R., & Laur, H. (1990a). Maximum a posteriori speckle filtering and first order texture models in sar images. In *Geoscience and remote sensing symposium, 1990. IGARSS '90. 'Remote sensing science for the nineties', 10th annual international*, pp. 2409–2412.

Lopes, A., Touzi, R., & Nezry, E. (1990b). Adaptive speckle filters and scene heterogeneity. *IEEE Transactions on Geoscience and Remote Sensing*, *28*, 992–1000.

Mallat, S. G. (1989a). Multifrequency channel decompositions of images and wavelet models. *IEEE Transactions on Acoustics, Speech and Signal Processing*, *37*, 2091–2110.

Mallat, S. G. (1989b). A theory for multiresolution signal decomposition: The wavelet representation. *IEEE Transactions on Pattern Analysis and Machine Intelligence*, *11*, 674–693.

Martin, F. J., & Turner, R. W. (1993). SAR speckle reduction by weighted filtering. *International Journal of Remote Sensing*, *14*, 1759–1774.

Moreira, A. (1991). Improved multilook techniques applied to sar and scansar imagery. *IEEE Transactions on Geoscience and Remote Sensing*, *29*, 529–534.

Novak, L. M., & Burl, M. C. (1990). Optimal speckle reduction in polarimetric SAR imagery. *IEEE Transactions on Geoscience and Remote Sensing*, *26*, 293–305.

Oliver, C., & Quegan, S. (2004). *Understanding synthetic aperture radar images*. Raleigh, NC 27613: SciTech Publishing.

Parrilli, S., Poderico, M., Angelino, C., & Verdoliva, L. (2012). A nonlocal SAR image denoising algorithm based on LLMMSE wavelet shrinkage. *IEEE Transactions on Geoscience and Remote Sensing*, *50*, 606–616.

Ponomaryov, V. I. (2007). Real-time 2D or 3D filtering using order statistics based algorithms. *Journal of Real-Time Image Processing*, *1*, 173–194. doi:10.1007/s11554-007-0021-5.

Porcello, L. J., Massey, N. G., Innes, R. B., & Marks, J. M. (1976). Speckle reduction in synthetic-aperture radars. *JOSA*, *66*, 1305–1311.

Qiu, F., Berglund, J., Jensen, J. R., Thakkar, P., & Ren, D. (2004). Speckle noise reduction in SAR imagery using a local adaptive median filter. *GIScience & Remote Sensing*, *41*, 244–266.

Shitole, S., De, S., Rao, Y. S., Mohan, B. K., & Das, A. (2014). Selection of suitable window size for speckle reduction and deblurring using SOFM in polarimetric SAR images. *Journal of the Indian Society of Remote Sensing*,. doi:10.1007/s12524-014-0403-7.

Shitole, S., Rao, Y. S., Mohan, B. K., Bhattacharya, A., & Das, A. (2013). Region growing based improved SAR speckle filter for

polarimetric data. In *Asia-Pacific conference on synthetic aperture radar (APSAR), 2013*, IEEE, pp. 517–520.

Simard, M., DeGrandi, G., Thomson, K. P., & Benie, G. B. (1998). Analysis of speckle noise contribution on wavelet decomposition of SAR images. *IEEE Transactions on Geoscience and Remote Sensing*, *36*, 1953–1962.

Sumantyo, J. T. S., & Amini, J. (2008). A model for removal of speckle noise in SAR images (ALOS PALSAR). *Canadian Journal of Remote Sensing*, *34*, 503–515.

Tan, C.-P., Koay, J.-Y., Lim, K.-S., Ewe, H.-T., & Chuah, H.-T. (2007). Classification of multi-temporal SAR images for rice crops using combined entropy decomposition and support vector machine technique. *Progress in Electromagnetics Research*, *71*, 19–39.

Walkup, J. F., & Choens, R. C. (1974). Image processing in signal-dependent noise. *Optical Engineering*, *13*, 133258–133258.

Wang, S., Liu, K., Pei, J., Gong, M., & Liu, Y. (2013). Unsupervised classification of fully polarimetric SAR images based on scattering power entropy and copolarized ratio. *IEEE Geoscience and Remote Sensing Letters*, *10*, 622–626.

Xiao, J., Li, J., & Moody, A. (2003). A detail-preserving and flexible adaptive filter for speckle suppression in SAR imagery. *International Journal of Remote Sensing*, *24*, 2451–2465.

Yamamoto, K., Yamaguchi, Y., Park, S.-E., Cui, Y., & Yamada, H. (2013). Comparison of speckle filtering methods for POLSAR analysis of earthquake damaged areas. *Asia-Pacific conference on synthetic aperture radar (APSAR), 2013*, IEEE, pp. 358–360.

Yueh, S., Kong, J., Jao, J., Shin, R., & Novak, L. (1989). K-distribution and polarimetric terrain radar clutter. *Journal of Electromagnetic Waves and Applications*, *3*, 747–768.